Remote Sensing of Aerosol Water Uptake

Gregory L. Schuster

Bing Lin

NASA Langley Research Center, Hampton, Virginia, USA

Oleg Dubovik

Laboratoire d'Optique Atmosphérique, Université de Lille 1/CNRS,

Villeneuve d'Ascq, France

An edited version of this paper was published and copyright (2009) by the American Geophysical Union:

Schuster, G. L., B. Lin, and O. Dubovik (2009), Remote sensing of aerosol water uptake, *Geophys. Res. Lett., 36,* L03814, doi:10.1029/2008GL036576.

Gregory L. Schuster, NASA Langley Research Center, Hampton, Virginia 23681, USA. (gregory.l.schuster@nasa.gov)

Aerosol water content is an important component of aerosol radiative forcing, but the effect of water uptake on aerosols throughout the atmospheric column is not monitored at the present time. We present a technique for retrieving the volume fraction of water in atmospheric aerosols, and apply the technique to the AERONET database. We estimate that the volume fraction of water and the geometric hygroscopic growth factor ($gHGF$) can be retrieved to within 0.3 using this retrieval. The growth factors we obtain are consistent with published measurements, and indicate that aerosol water uptake is high in humid continental regions ($gHGF \sim 1.3$ along the U.S. East Coast in August) and low in regions dominated by desert dust ($gHGF \sim 1.04$ in Saudi Arabia).

1. Introduction

Atmospheric aerosols include a hygroscopic component that absorbs water and shifts particles to more efficient scattering sizes [*Hegg et al.*, 1993]. This aerosol water uptake has a significant impact on visibility [*Sloane and White*, 1986] and is a key component of the aerosol direct effect in regions with elevated relative humidities. Aerosol water content is strongly dependent upon aerosol composition and relative humidity (RH), and may constitute a significant fraction of the aerosol mass [even at relative humidities below 60%; *Pilinis and Seinfeld*, 1989]. Consequently, aerosol water content is problematic for model computations of aerosol radiative forcing, and there is a need for continuous monitoring of the aerosol liquid water content.

The aerosol real refractive index reveals information about the water content of internally mixed aerosols (i.e., aerosol mixtures with refractive indices close to 1.33 have an abundance of water, while those with refractive indices close to 1.57 are dry). Remote sensing technology has evolved to the point where we can now retrieve the aerosol real refractive index using passive radiometric measurements [*Dubovik and King*, 2000; *Chowdhary et al.*, 2001] and lidar measurements [*Muller et al.*, 2004]. Soon, the aerosol real refractive index will also be available from satellite data products [*Mishchenko et al.*, 2007]. We demonstrate how the aerosol real refractive index may be used to retrieve the aerosol water fraction, and provide examples of the retrieval using the AERONET product [which has been available and scrutinized for many years; *Holben et al.*, 1998; *Dubovik et al.*, 2000].

2. Retrieval of aerosol water fraction from the real refractive index

The sensitivity of aerosol water fraction (f_w) to the real refractive index is shown for a variety of water-aerosol mixtures in Figure 1. Three of the mixtures (sea salt, ammonium sulfate, ammonium nitrate) contain a water-soluble aerosol. A fourth mixture contains an insoluble aerosol with a refractive index of $m = 1.57 + 0.002i$, which is the highest refractive index for dust that we found in the literature that is also exclusive of high amounts of hematite or geothite. We used partial molar refraction for the soluble aerosol mixtures [*Lacis, http://gacp.giss.nasa.gov/data_sets/; Tang and Munkelwitz*, 1994], and the Maxwell-Garnett effective medium approximation for the mixtures with insoluble aerosols [*Bohren and Huffman*, 1983].

The soluble aerosols in Figure 1 indicate similar refractive indices for similar aerosol mixing ratios, even though the dry refractive indices can be quite different (note the appropriate symbols for the dry soluble aerosols at the bottom of the plot). Hence, the aerosol water fraction can be derived from the mixture real refractive index if the aerosols are known to be one of the common soluble aerosols. However, most atmospheric aerosol mixtures will include a combination of both soluble and insoluble aerosols (as well as water), and will therefore lie between the solid and dashed lines of Figure 1 (as long as the average real refractive index of the insoluble component lies in the range of 1.47–1.57). Consequently, three aerosol components are required for retrieving the aerosol water fraction.

We retrieve the aerosol water fraction by adjusting f_w in a theoretical mixture of water, soluble, and insoluble species until the refractive index of the mixture corresponds to a minimum χ^2-fit of the refractive indices provided by remote sensing [similar to *Schuster*

et al., 2005]. Since there are only two pieces of information available (real refractive index and conservation of mass) for this three-component retrieval, we constrain the insoluble/soluble aerosol ratio using the empirical relation:

$$f_i/f_s = R_{ks}[293.33(\overline{m_r} - 1.33)^3 + 0.01], \quad (1)$$

which prescribes the aerosol hygroscopicity. Here, f_i is the dry volume fraction of insoluble aerosols, f_s is the dry volume fraction of soluble aerosols, R_{ks} is the climatological value for f_i/f_s [*Kandler and Schütz*, 2007], and $\overline{m_r}$ is the average real refractive index at the available wavelengths. This constraint was adjusted to match the hygroscopic growth at the ARM SGP site [*Sheridan et al.*, 2001], and produces a maximum insoluble fraction of 80% for all retrievals at the 53 AERONET that we tested; this is consistent with the maximum insoluble fraction deduced by *Zhang et al.* [1993]. If the imaginary refractive index is also known (as at the AERONET sites), then we can also infer black carbon concentration through a χ^2–iteration process of the imaginary refractive index [*Schuster et al.*, 2005].

2.1. Retrieval of other wet and dry aerosol properties

Once the volume fraction of water in the aerosol mixture (f_w) has been obtained through the χ^2-iteration process described above, we can compute a number of hygroscopic aerosol properties. For instance, the geometric hygroscopic growth of aerosols may be expressed as

$$gHGF = \frac{R}{\widehat{R}} = \frac{1}{\sqrt[3]{1 - f_w}}, \quad (2)$$

where R is the aerosol radius at ambient RH and $\widehat{R}$ is the corresponding dry radius (at $RH = 0$). If the column aerosol size distribution is also known ($\frac{dV}{d\ln r}$), then the aerosol liquid water path may be expressed as

$$LWP_a = f_w \rho_w \int \frac{dV}{d\ln r} d\ln r, \tag{3}$$

where ρ_w is the density of water. Conservation of mass provides the dry aerosol fraction ($f_d = 1 - f_w$) and the dry size distribution, which is more useful for comparisons with in situ measurements than the standard AERONET product.

2.2. Uncertainty assessment

Figure 1 demonstrates the uncertainty of the retrieval, where we show the retrieval at two AERONET sites with the crosses. Here, we use ammonium nitrate for the soluble component, dust for the insoluble component [*Sinyuk et al.*, 2003; *Dubovik et al.*, 2002], and a black carbon component [refractive index $m_{bc} = 1.95 - 0.79i$ and density $\rho_{bc} = 1.8$ g cm^{-3}, per *Bond and Bergstrom*, 2006]. Throughout this article we use AERONET version 2 dataset and quality level 2.0 or 1.5.

The shaded area represents results for all possible mixtures of ammonium nitrate and water with up to 80% insoluble aerosols (i.e., $f_i/f_s \leqslant 4$) and refractive indices of 1.45–1.61. This range of refractive indices encompasses dust and most organic carbon [*Krekov*, 1993; *Dick et al.*, 2007]. Note that the crosses have a maximum deviation of $\delta f_w \sim 0.3$ from the edges of the shaded area, which estimates the maximum uncertainty of the retrieval. A similar plot of $gHGF$ vs. refractive index indicates that the maximum variability in $gHGF$ varies from $\delta(gHGF) \leqslant 0.17$ when $gHGF \leqslant 1.11$ to $\delta(gHGF) \geqslant 0.55$ when

$gHGF \geqslant 1.85$ (not shown). The maximum uncertainty of both f_w and $gHGF$ increases by 0.1 in smoky regions with 10% black carbon (if the black carbon fraction is not retrieved by some other means). Finally, the maximum uncertainty increases if the insoluble aerosols are dominated by organic carbon mixtures with refractive indices significantly less than 1.45.

3. Aerosol Growth and Relative Humidity

Since this retrieval does not utilize RH as an input parameter, we test the fidelity of the retrieval by observing the response of aerosol hygroscopic growth to RH. This is shown in Figure 2, where we plot monthly climatology of retrieved aerosol water fraction and surface RH at three sites (AERONET all-points level 1.5 dataset, restricted to solar zenith angles $> 50^\circ$ and $AOD_{440} > 0.1$). The symbols in Figure 2 are sized relative to the aerosol optical depth, and the whiskers represent two standard deviations of the mean values.

Figure 2 shows that f_w trends as expected with RH, with the largest water fractions occurring for the highest optical depths and relative humidities at both the Bondville and COVE sites; the Boulder site is a dry location with low RH, and consequently shows little water uptake. The retrievals are also consistent with the dashed line in Figure 2, which is a parameterization of in situ measurements obtained in Tennessee during the Southeastern Aerosol Visibility Study [SEAVS, *Kreisberg et al.*, 2001]. Variability of water uptake is shown by the shaded area of Figure 2, which represents the range of values measured by *Khlystov et al.* [2005] over a 12-month period near downtown Pittsburgh, Pennsylvania.

4. LWP_a and Aerosol Composition

The volume and mass of aerosols increases as hygroscopic particles absorb water, so LWP_a (Equation 3) should be well-correlated with the volume concentration of hygroscopic aerosols and less well-correlated with hydrophobic aerosols. At many continental locations, the fine mode is composed of highly hygroscopic pollution aerosols or moderately hygroscopic biomass burning aerosols, while the coarse mode is dominated by hydrophobic dust. These composition differences offer an opportunity to test the fidelity of the retrieval.

We examine the relationship between LWP_a and aerosol composition in Table 1, which shows the coefficient of determination (R^2) for the fine and coarse volume concentrations at several AERONET sites. All of the sites in Table 1 indicate much higher R^2 values for the fine mode than for the coarse mode (with the exception of Ouagadougou), consistent with our expectations of the previous paragraph. More broadly, R^2_{fine} is almost always greater than R^2_{crs} at all of the AERONET sites that we tested (minimum of 100 retrievals each); only 15 of the 351 sites (4%) have $R^2_{crs} > R^2_{fine}$, and these sites are almost exclusively the dust sites of Northern Africa and some coastal sites.

Indeed, Ouagadougou is an anomaly in Table 1 (with high R^2 values for both the fine and coarse modes), but it is not atypical for the AERONET sites in Northern Africa, which are dominated by year-round dust and a long biomass burning season. The cause of the high R^2_{crs} values in Northern Africa is unknown at this point, but we emphasize that high R^2 values do not necessarily indicate high aerosol water fractions. Rather, high R^2 values indicate the degree to which changes in the aerosol volume concentration are

associated with changes in LWP_a. It is possible that moderately hygroscopic biomass burning aerosols are mixing with the dust aerosols in similar proportions for both the fine and coarse modes in Northern Africa (median mode separation radius: 0.44μm), which would result in similar R^2 values for both modes.

5. Regional Climatology

It is useful to place these results in the context of previous studies, even though water uptake is almost exclusively reported at a reference RH (80–90%) rather than the ambient conditions of our retrievals. Previous aerosol hygroscopic growth measurements have indicated that aerosol hygroscopicity can be classified into several categories: particles are "nearly-hydrophobic" when $gHGF$=1.0–1.11, "less-hygroscopic" when $gHGF$ =1.11–1.33, "more-hygroscopic" when $gHGF > 1.33$, and as "sea-salt" in marine airmasses when $gHGF > 1.85$ [all at a reference RH of 90%; *Swietlicki et al.*, 2008]. Hence, desert dust aerosols are dominated by nearly-hydrophobic particles, biomass burning aerosols are characterized by less-hygroscopic particles, and polluted continental sites tend to be dominated by more-hygroscopic particles. We applied our retrieval of $gHGF$ to all available AERONET refractive index retrievals and computed column-effective monthly averages (requiring at least 10 retrievals for each month); global results for the months of February and August are shown in Figure 3, and the locations of some of the sites that we discuss are presented in Table 1.

During the month of August (right panel), urban sites at humid locations tend to have the highest $gHGF$, as denoted by the blue circles along eastern U.S.A., Europe, and the east coast of Asia. Polluted East Asian sites located inland have less water uptake than the

urban sites in the eastern U.S. (i.e., $gHGF = 1.21 \pm 0.04$ at Beijing, 1.32 ± 0.05 at GSFC), but the RH is lower at the Asian locations as well. Arid sites with predominantly dust aerosols in the Middle East and Northern Africa have the lowest water uptake ($gHGF = 1.03 \pm 0.004$ at Solar Village, 1.04 ± 0.02 at Ouagadougou), while the rural biomass burning sites of Southern Africa and South America indicate slightly greater water uptake than the dust sites ($gHGF = 1.07 \pm 0.01$ at Mongu, 1.11 ± 0.02 at Cuiaba-Miranda). These results are consistent with the hygroscopicity classification scheme described above, with the possible exception of Mongu (which might be construed as nearly-hydrophobic dust aerosols rather than less-hygroscopic biomass burning aerosols). However, the average RH in Mongu is 27% in August (weatherreports.com), so it is very likely that the Mongu aerosols would grow to the less-hygroscopic category if they were subjected to the 90% reference RH mentioned above.

There are far fewer sites with available data during February in Figure 3 (left panel) because the AERONET level 2.0 dataset is restricted to $AOD_{440} \geqslant 0.4$. The East Asian sites have less water uptake in February than in the humid conditions of August. The North African sites have greater water uptake in February than in August because of wintertime biomass burning aerosols in that region (i.e., $gHGF = 1.17 \pm 0.02$ in February at Ouagadougou, 1.04 ± 0.02 in August). The desert sites of the Middle East also indicate slightly greater water uptake in February than in August ($gHGF = 1.06 \pm 0.01$ at Solar Village in February, and $gHGF = 1.03 \pm 0.004$ in August), but the RH is also higher in February.

Finally, we also computed column-effective growth factors obtained at nine AERONET sites deployed for the Smoke, Clouds, and Radiation-Brazil (SCAR-B) field mission (Alta Floresta, Brasilia, Campo Grande, Cuiaba, El Refugio, Ji Parana, Santarem, Tukurui, and Uberlandia); we obtained a median value of $gHGF = 1.04$, which is midrange of the values that *Kotchenruther and Hobbs* [1998] measured using in situ instrumentation (i.e., $gHGF = 1$–1.1).

6. Discussion

One shortcoming of this retrieval is that aerosols of all sizes are assumed to grow at the same rate (or equivalently, have the same composition). Although it is reasonable to expect similar water uptake for aerosol with radii greater than 0.05 μm in the accumulation mode [*Swietlicki et al.*, 2008], aerosols in the coarse mode are generally composed of different species than the accumulation mode, so they have different water uptake. The water uptake of this retrieval represents a value that is intermediate of either mode; if a dominant mode exists, then the retrieved water is more representative of the dominant mode than the secondary mode.

Aerosol mixtures with real refractive indices greater than $\sim$1.53 are required to be completely dry with this retrieval (Figure 1). This is a direct result of the empirical relationship (Equation 1) that was adjusted to match the hygroscopic growth at the ARM SGP site [*Sheridan et al.*, 2001]. We note that although Equation 1 is appropriate for the ARM SGP site and perhaps other continental sites as well, it may not be appropriate for all locations. Nonetheless, it seems reasonable that a range of large refractive indices

($\gtrsim$1.53) correspond to aerosol mixtures with little or no water. Further testing at a multitude of AERONET sites is necessary.

Like most radiometric retrievals, statistically averaged values (like we have shown here) will produce more robust results than individual retrievals. Indeed, we have not rigorously validated this retrieval on a case-by-case basis at the present time; additional in situ measurements of $gHGF$ and f_i/f_s at key AERONET sites would be helpful for this task. Additional studies of the relationship between aerosol water fraction and the real refractive index for laboratory and atmospheric aerosol mixtures (i.e., Figure 1) would also be helpful for improving and adjusting this technique on a regional basis.

7. Conclusion

We presented a method for retrieving the aerosol water uptake from the aerosol real refractive index, and applied it to the column-effective AERONET retrievals. We estimate the aerosol water fraction and geometric hygroscopic growth factor are accurate to better than 0.3, but this retrieval has not been fully validated at the present time. Nonetheless, this technique is consistent with measurements obtained in Tennessee during SEAVS and Brazil during SCAR-B. The results are also consistent with expectations on a regional and compositional basis, indicating the largest growth factors for polluted regions with high humidities and the smallest growth factors for regions dominated by desert dust.

Acknowledgments.

We appreciate the efforts of the 53 AERONET and PHOTONS (Service d'Observation from LOA/USTL/CNRS) principal investigators and the entire AERONET/PHOTONS teams. Relative humidity data are funded by the NASA Earth Observing System project

at the COVE site and by NOAA Global Monitoring Division for the Bondville and Boulder sites. This work was funded by NASA SMD/ESD and the CERES project.

References

Bohren, C., and D. Huffman (1983), *Absorption and scattering of light by small particles*, Wiley.

Bond, T., and R. Bergstrom (2006), Light absorption by carbonaceous particles: An investigative review, *Aerosol Sci. Technol.*, *40*(1), 27–67.

Chowdhary, J., B. Cairns, M. Mishchenko, and L. Travis (2001), Retrieval of aerosol properties over the ocean using multispectral and multiangle photopolarimetric measurements from the Research Scanning Polarimeter, *Geophys. Res. Lett.*, *28*(2), 243–246.

Dick, W. D., P. J. Ziemann, and P. H. McMurry (2007), Multiangle light-scattering measurements of refractive index of submicron atmospheric particles, *Aerosol Sci. Technol.*, *41*(5), 549–569.

Dubovik, O., and M. King (2000), A flexible inversion algorithm for retrieval of aerosol optical properties from sun and sky radiance measurements, *J. Geophys. Res.*, *105*(D16), 20,673–20,696.

Dubovik, O., A. Smirnov, B. Holben, M. King, Y. Kaufman, T. Eck, and I. Slutsker (2000), Accuracy assessments of aerosol optical properties retrieved from Aerosol Robotic Network (AERONET) sun and sky radiance measurements, *J. Geophys. Res.*, *105*(D8), 9791–9806.

Dubovik, O., B. Holben, T. Eck, A. Smirnov, Y. Kaufman, M. King, D. Tanre, and I. Slutsker (2002), Variability of absorption and optical properties of key aerosol types observed in worldwide locations, *J. Atmos. Sci.*, *59*, 590–608.

Hegg, D., T. Larson, and P. Yuen (1993), A theoretical study of the effect of relative humidity on light scattering by tropospheric aerosols, *J. Geophys. Res.*, *98*(D10), 18,435–18,439.

Holben, B., et al. (1998), AERONET – A federated instrument network and data archive for aerosol characterization, *Remote Sens. Environ.*, *66*, 1–16.

Kandler, K., and L. Schütz (2007), Climatology of the average water-soluble volume fraction of atmospheric aerosol, *Atmospheric Research*, *83*, 77–92.

Khlystov, A., C. O. Stanier, S. Takahama, and S. N. Pandis (2005), Water content of ambient aerosol during the Pittsburgh Air Quality Study, *J. Geophys. Res.*, *110*, D07S10, doi:10.1029/2004JD004651.

Kotchenruther, R., and P. Hobbs (1998), Humidification factors of aerosols from biomass burning in Brazil, *J. Geophys. Res.*, *103*(D24), 32,081–32,089.

Kreisberg, N., M. Stolzenburg, S. Hering, W. Dick, and P. McMurry (2001), A new method for measuring the dependence of particle size distributions on relative humidity, with application to the Southeastern Aerosol Visibility Study, *J. Geophys. Res.*, *106*(D14), 14,935–14,949.

Krekov, G. (1993), *Aerosol Effects on Climate*, chap. 1, pp. 9–64, University of Arizona Press.

Mishchenko, M., et al. (2007), Accurate monitoring of terrestrial aerosols and total solar irradiance, *Bull. Amer. Meteor. Soc.*, *88*(5), 677–691.

Muller, D., I. Mattis, A. Ansmann, B. Wehner, D. Althausen, U. Wandinger, and O. Dubovik (2004), Closure study on optical and microphysical properties of a mixed urban and Arctic haze air mass observed with Raman lidar and Sun photometer, *J. Geophys. Res.*, *109*, D13206, doi:10.1029/2003JD004200.

Pilinis, C., and J. Seinfeld (1989), Water content of atmospheric aerosols, *Atmos. Environ.*, *23*(7), 1601–1606.

Schuster, G. L., O. Dubovik, B. N. Holben, and E. E. Clothiaux (2005), Inferring black carbon content and specific absorption from Aerosol Robotic Network (AERONET) aerosol retrievals, *J. Geophys. Res.*, *110*, D10S17, doi:10.1029/2004JD004548.

Sheridan, P., D. Delene, and J. Ogren (2001), Four years of continuous surface aerosol measurements from the Department of Energy's Atmospheric Radiation Measurement Program Southern Great Plains Cloud and Radiation Testbed site, *J. Geophys. Res.*, *106*(D18), 20,735–20,747.

Sinyuk, A., O. Torres, and O. Dubovik (2003), Combined use of satellite and surface observations to infer the imaginary part of refractive index of Saharan dust, *Geophys. Res. Lett.*, *30*(2), 1081, doi:10.1029/2002GL016189.

Sloane, C., and W. White (1986), Visibility: An evolving issue, *Environ. Sci. Technol.*, *20*(8), 760–766.

Swietlicki, E., et al. (2008), Hygroscopic properties of submicrometer atmospheric aerosol particles measured with H-TDMA instruments in various environments—a review, *Tel-*

lus, *60B*, 432–469.

Tang, I., and H. Munkelwitz (1994), Water activities, densities, and refractive indices of aqueous sulfates and sodium nitrate droplets of atmospheric importance, *J. Geophys. Res.*, *99*(D9), 18,801–18,808.

Zhang, X., P. McMurry, S. Hering, and G. Casuccio (1993), Mixing characteristics and water content of submicron aerosols measured in Los Angeles and at the Grand Canyon, *Atmos. Environ.*, *27A*(10), 1593–1607.

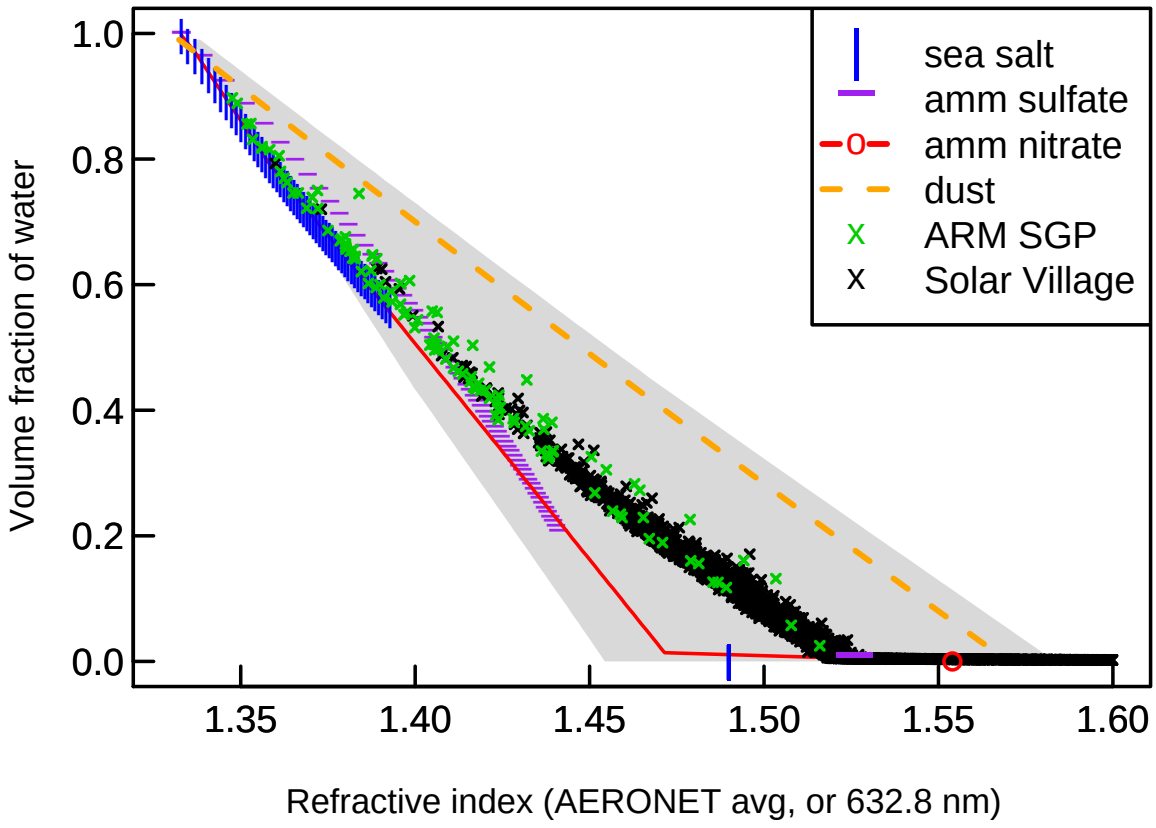

Figure 1. Water fractions for two-component aerosol mixtures as a function of the real refractive index. Also shown are the results from the retrieval discussed in this paper, as applied to the Cart_Site and Solar Village AERONET sites (all-points, level 2.0 dataset).

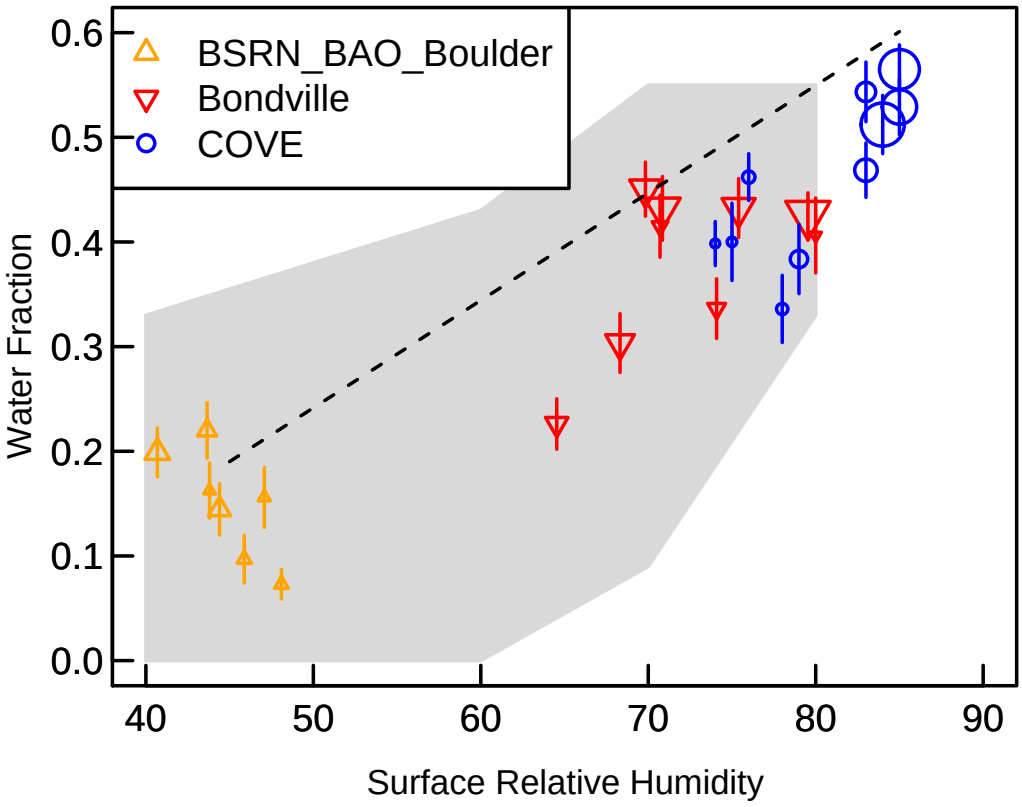

Figure 2. Monthly averaged climatology of retrieved water uptake at three AERONET sites vs. surface RH, which is an independent measurement. (all-points, level 1.5 dataset.)

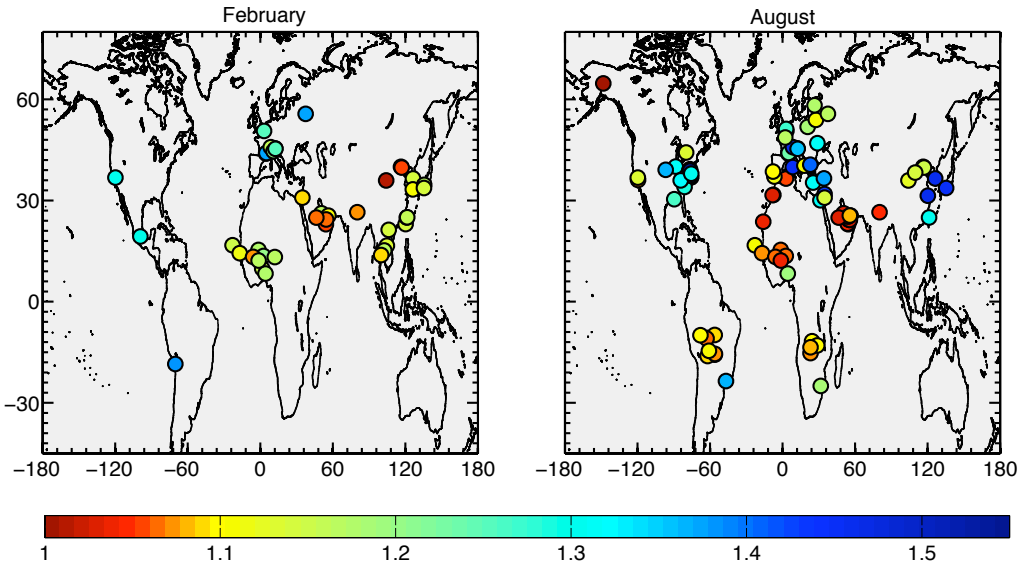

Figure 3. February and August climatology of the geometric hygroscopic growth factor ($gHGF$) at all AERONET sites. (AERONET all-points, level 2.0 dataset, minimum of 10 retrievals.)

Table 1. Coefficient of determination (R^2) of aerosol liquid water path with fine mode concentration and coarse mode concentration. The ratio of average fine volume fraction to total volume fraction is also shown. (AERONET all-points, level 1.5 dataset.)

Location	Lon.	Lat.	R^2_{fine}	R^2_{crs}	$\overline{V_f}/\overline{V_T}$
Solar Village	46.4	24.9	0.323	0.046	0.10
Ouagadougou	-1.4	12.2	0.434	0.456	0.11
Sede Boker	34.8	30.9	0.476	0.059	0.20
Cairo EMA	31.3	30.1	0.646	0.006	0.29
Boulder (BSRN)	-105.0	40.0	0.613	0.017	0.38
Beijing	116.4	40.0	0.458	0.001	0.40
Cuiaba-Miranda	-56.0	-15.7	0.489	0.030	0.54
Bondville	-88.4	40.0	0.721	0.068	0.55
Mongu	23.2	-15.3	0.311	0.154	0.60
COVE	-75.7	36.9	0.704	0.132	0.62
GSFC	-76.8	39.0	0.734	0.089	0.64